Investigation of the low- and medium-spin level structure in ^{77}As

A. K. Mondal,[*] A. Chakraborty,[†] K. Mandal,[‡] U. S. Ghosh, Aniruddha Dey, Saumyajit Biswas,[§] and B. Mukherjee
Department of Physics, Siksha Bhavana, Visva-Bharati University, Santiniketan, West Bengal 731 235, India

Krishichayan
Department of Physics, Duke University, Durham, North Carolina 27708, USA and Triangle Universities Nuclear Laboratory, Durham, North Carolina 27708, USA

S. Chatteerjee, S. K. Das, S. Samanta, R. Raut, and S. S. Ghugre
UGC-DAE Consortium for Scientific Research, Sector III, LB-8, Bidhan Nagar, Kolkata 700 106, India

S. Mukhopadhyay
Nuclear Physics Division, Bhabha Atomic Research Centre, Trombay, Mumbai 400 085, India and Homi Bhabha National Institute, Training School Complex, Anushaktinagar, Mumbai 400 094, India

S. Rajbanshi
Department of Physics, Presidency University, Kolkata 700 073, India

R. Banik, S. Bhattacharyya, S. Nandi, S. Chakraborty, S. Bhattacharya, and G. Mukherjee
Variable Energy Cyclotron Centre, Sector I/AF, Bidhan Nagar, Kolkata, West Bengal 700 064, India and Homi Bhabha National Institute, Training School Complex, Anushaktinagar, Mumbai 400 094, India

S. Ali
Department of Physics, Government General Degree College at Pedong, Kalimpong, West Bengal 734 311, India

A. Goswami[‖]
Saha Institute of Nuclear Physics, I/AF, Bidhan Nagar, Kolkata, West Bengal 700 064, India

R. Chakrabarti
Department of Physics, University of Mumbai, Vidyanagari, Mumbai 400 098, India

A. Kumar
Department of Physics, Banaras Hindu University, Varanasi 221 005, India

R. Goswami
B.P. Poddar Institute of Management and Technology, Kolkata 700 052, India

(Received 1 February 2023; accepted 9 June 2023; published 30 June 2023)

The low- and medium-spin level structure of ^{77}As nucleus has been investigated using the ^{76}Ge(α, $p2n$) fusion evaporation reaction and the standard in-beam γ ray spectroscopic technique. The deexciting γ rays were detected with the Indian National Gamma Array spectrometer comprising Clover and LEPS detectors. The previously known $9/2^+$ yrast positive-parity band, based on the $\pi(g_{9/2})$ configuration, has been extended to the excitation energy of $E_x \approx 7.5$ MeV with $J^\pi = (33/2^+)$. An extension of the high-lying negative-parity band, based on the $\pi[(g_{9/2})] \otimes \nu[(g_{9/2})(fp)]$ configuration, has been made up to $E_x \approx 5.1$ MeV, $J^\pi = (25/2^-)$.

[*]Also at the Department of Physics, Bolpur College, Bolpur, West Bengal 731 204, India.
[†]anagha.chakraborty@visva-bharati.ac.in
[‡]Also at the Department of Physics, Chandidas Mahavidyalaya, Khujutipara, West Bengal 731 215, India.
[§]Also at Department of Physics, Murshidabad College of Engineering and Technology, Banjetia, West Bengal 742 102, India.
[‖]Deceased.

The yrast positive-parity $\alpha = -1/2$ signature partner band has newly been identified and the occurrence of large signature splitting associated with the partner bands have been observed. A quasi-γ vibrational band structure built on the nonyrast $13/2^+$ state has also newly been established. The experimental findings have been interpreted on the basis of the predicted results from the total Routhian surface, particle plus triaxial-rotor model, and shell-model calculations. The band crossing phenomena correlated to the $\nu(g_{9/2})$ alignment and the perseverance of triaxial shape up to the highest observed excitation regime of the $9/2^+$ yrast positive-parity band have been discussed. The evidence for the possible onset of the stapler-like mechanism prevailing in the high-lying negative-parity band structure are presented.

DOI: 10.1103/PhysRevC.107.064320

I. INTRODUCTION

The odd-mass nuclei in the $A \approx 70$–80 mass regions exhibit a variety of nuclear excitation phenomena such as the occurrence of large signature splitting, signature inversion, band crossing associated with quasiparticle alignment, shape coexistence, shears, and stapler-like mechanisms associated with the dipole bands [1,2], etc. In this context, the odd-mass ^{77}As nucleus, lying within the periphery of $N = 50$ shell closure, is expected to be an ideal candidature for investigating these phenomena. In fact, one can expect a competition between the single-particle and collective degrees of freedom arising because of the availability of few valence nucleons. It is also interesting to note that the $\pi(g_{9/2})$ excitation leads to the formation of the yrast $9/2^+$ isomeric state in ^{77}As. Such an isomeric state and the yrast $E2$ band structure built on the isomeric state are found to be systematically present in the isotopes and isotones of ^{77}As [1,3]. Also, the previous investigations have shown large signature splitting among the yrast $g_{9/2}$ positive-parity partner bands of a few $N = 44$ isotones of ^{77}As [1]. As the unfavored ($\alpha = -1/2$) signature partner bands are weakly populated, they are difficult to observe experimentally and hence remain unidentified in most of the cases. This is probably the cause for the signature partner bands not being identified in ^{77}As by the previous investigators, along with the fact that the previous studies [4] were carried out with the gamma arrays consisting of a few detectors only. In addition, the band-crossing phenomena, due to the $\nu(g_{9/2})^2$ alignment, which is expected to occur in the yrast positive-parity band of ^{77}As could not be studied in the previous investigation due to the unavailability of data up to the expected regime of crossing frequency [4].

It is worthwhile mentioning that the magnetic rotation bands have previously been observed in several nuclei belonging to $A \approx 80$ region [2,5]. The presence of the high-j intruder $g_{9/2}$ orbitals are considered to be the cause for the onset of a shears-like mechanism [6], which subsequently leads to the formation of magnetic rotation bands. An alternate method such as a "stapler-like" mechanism for generating the angular momentum in the high-lying negative-parity dipole band structure is also proposed, and the same has been observed in ^{75}As [7]. In fact, the recent investigation of the level structure of ^{78}As by our group has demonstrated the possibility for the presence of such type of stapler-like mechanism prevailing in the high-lying negative-parity dipole band structure of ^{78}As [2]. Hence, it would be interesting to identify such negative-parity band structure in ^{77}As and characterize the mechanism for generating the angular momentum associated with the underlying band structure.

With the aforesaid motivations, a detailed experimental investigation has been carried out to study the different excitation modes in ^{77}As. It is to be pointed out here that the previous experimental studies on the low-lying level structure of ^{77}As were carried out by several groups using a variety of probes. The investigations using the transfer reactions, ^{76}Ge(^{3}He, d) [8,9], ^{78}Se(d, ^{3}He) [10], and ^{78}Se(pol d, ^{3}He) [11] and the β^- decay of ^{77}Ge [12–16] were carried out to identify the low-lying levels of ^{77}As. Definitive spin-parity assignments for some of the low-lying levels of ^{77}As could be made possible from these investigations, and the level scheme was extended up to $E_x \approx 4$ MeV. The previous in-beam γ ray spectroscopic study for the excited levels of ^{77}As was carried out by Döring *et al.* [4] using the ^{76}Ge(α, $p2n$)^{77}As reaction at the incident beam energies of 32, 36, and 40 MeV. A total of six Ge detectors along with two ΔE-E telescopes were used for the measurement. The extension of the level scheme up to $E_x = 4.4$ MeV could be made following the spectroscopic data obtained from the measurement. This is found to be the only in-beam γ-ray spectroscopic measurement for ^{77}As available in the literature prior to the present investigation. The present investigation on ^{77}As has been carried out using the fusion evaporation reaction ^{76}Ge(α, $p2n$) at the incident beam energy of 40 MeV. A modest array of gamma detectors with good resolving power and high detection efficiency has been used. The experimental details and the results along with the necessary interpretations are provided in the follow-up sections.

II. EXPERIMENTAL PROCEDURE AND DATA ANALYSIS

The 40 MeV α beam used for the present experiment was delivered by the K-130 Cyclotron machine at the Variable Energy Cyclotron Centre (VECC), Kolkata. The target comprising of 94% enriched ^{76}Ge isotope was prepared at the target laboratory of VECC through the centrifuge process. The enriched ^{76}Ge oxide powder was deposited on the Mylar backing. The thickness of the target thus prepared was found to be about 2 mg/cm^2. For the enhancement in the production yields of the residual nuclei, the experiment was carried out using two such targets stacked together. The deexciting γ rays from the excited states of the residual nuclei were detected using the Indian National Gamma Array (INGA). The array was comprised of six Compton-suppressed clover detectors and one low energy photon spectrometer (LEPS).

The clover detectors were arranged in the form of two groups: four detectors were placed at 90° and two were at 125°, with respect to the beam direction. The single LEPS used during the experiment was placed at 40°. The data were recorded using a 250 MHz 12-bit PIXIE-16 digital data-acquisition system [17]. A total of about 2.8×10^8 $\gamma\gamma$ coincidence events were recorded during the experiment. The Linux-based code IUCPIX, developed at the UGC-DAE CSR, Kolkata Centre [17] was used for carrying out the off-line data sorting process. The required energy and efficiency calibrations of the detectors were performed using the γ-ray transitions from the ^{152}Eu and ^{133}Ba radioactive sources. The conventional $\gamma\gamma$ symmetric and asymmetric matrices were constructed from the acquired data in order to perform a detailed off-line analysis. The RADWARE [18] and TV [19] software packages were used extensively for the subsequent spectral analysis.

The spin assignments of the excited levels of ^{77}As were performed from the analysis of directional correlations of γ rays deexciting from the oriented states (DCO) ratio method [20,21]. The measurement of the DCO ratio R_{DCO} is based on the ratio of intensities of a γ ray obtained from the angle-dependent $\gamma\gamma$ coincidence spectra. The DCO ratios of the concerned γ transitions have been extracted in the present work using the following definition:

$$R_{DCO} = \frac{I_{\gamma_1} \text{ at } 125^\circ \text{ gated with } \gamma_2 \text{ at } 90^\circ}{I_{\gamma_1} \text{ at } 90^\circ \text{ gated with } \gamma_2 \text{ at } 125^\circ}. \quad (1)$$

To extract R_{DCO} values following Eq. (1), the $\gamma\gamma$ coincidence data have been sorted into an asymmetric matrix with one of its axis corresponding to the events recorded by 90° detectors and the other axis corresponding to the events recorded by 125° detectors. The stretched and pure $E2$ and $E1$ transitions are preferable as gating transitions for extracting the R_{DCO} values of the transitions with unknown multipolarities. In this context, an effort has been made to extract the R_{DCO} values by setting gates on the several known $E2$ and $E1$ transitions. However, the transitions with the known $\Delta J = 1$, $M1 + E2$ multipolarities have also been used as the gates in extracting the R_{DCO} values of some specific transitions where the use of gates with the pure $E2$ and $E1$ transitions could not be made possible. The R_{DCO} values of the transitions extracted from different gating transitions are presented in Table I and pictorially represented in Fig. 1. The R_{DCO} values obtained by setting the gates on $\Delta J = 1$ transitions is shown in Fig. 1(a); whereas Fig. 1(b) represents the values extracted from the stretched $E2$ gates. The $\Delta J = 1$ and $\Delta J = 2$ lines have been drawn to guide the eye. The $\Delta J = 1$ and $\Delta J = 2$ lines of Figs. 1(a) and 1(b) have been drawn through the weighted mean of the R_{DCO} values of several well-known $E1$ and $E2$ transitions of ^{77,78}Se determined by using the known stretched and pure $E2$ and $E1$ gating transitions. The weighted mean values thus obtained are found to be 0.65 ± 0.03 (for $\Delta J = 1$ transitions with $E2$ gates) and 1.46 ± 0.03 (for $\Delta J = 2$ transitions with $E1$ gates). The weighted R_{DCO} values correspond to a value of $\sigma/J = 0.35$ as obtained by using the ANGCOR code [22]. It is further to be noted that for pure nonstretched $\Delta J = 0$ transitions, the expected R_{DCO} values will be close to unity when a $\Delta J = 2$ transition is used as the gate.

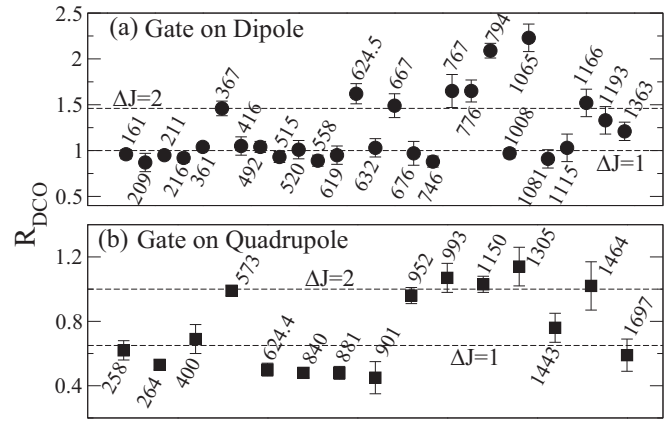

FIG. 1. The experimental R_{DCO} values extracted for the transitions belonging to ^{77}As.

The parity of the excited levels in ^{77}As have been assigned from the linear polarization asymmetry measurements [23] of the γ rays decaying from the concerned levels. The data from the four clover detectors located at 90° were used for this purpose. The electric and magnetic nature of the observed transitions have been assigned using the extracted value of polarization asymmetry (Δ_{asym}) defined as

$$\Delta_{\text{asym}} = \frac{[a(E_\gamma)N_\perp] - N_\parallel}{[a(E_\gamma)N_\perp] + N_\parallel}, \quad (2)$$

where $N_\perp$ and $N_\parallel$ are the respective counts of the scattered photons in the perpendicular and parallel planes with respect to the reaction plane. The term $a(E_\gamma)$ is defined as $a(E_\gamma) = N_\parallel$ (unpolarized)/$N_\perp$ (unpolarized), and it represents the geometrical asymmetry correction factor. In the present experiment, the value of $a(E_\gamma)$ has been determined from the best fit to the data obtained from the unpolarized ^{152}Eu radioactive source following the equation $a(E_\gamma) = a_0 + a_1 E_\gamma$. The values of the coefficients thus obtained are, $a_0 = 1.002(10)$ and $a_1 \approx 10^{-6}$. As the extracted value of a_1 is negligibly small, the same has not been considered in the subsequent polarization asymmetry calculations. The required perpendicular ($N_\perp$) and parallel ($N_\parallel$) scattered components of the concerned in-beam γ rays were obtained from the two asymmetric matrices. The matrices were constructed considering the parallel or perpendicular scattered events recorded by the 90° clover detectors along one axis, and the events recorded by all the other detectors along the other axis. As an electric transition would preferentially scatter in the perpendicular direction, a positive Δ_{asym} value is expected in general for such electric transitions. The negative value of the Δ_{asym} parameter corresponds to the magnetic character of the scattered γ ray. A near-zero value of the Δ_{asym} indicates mixed multipole character of the concerned transition. However, for a pure $\Delta J = 0$ transition, the electric (magnetic) nature of a γ ray corresponds to a negative (positive) value of the Δ_{asym} parameter. The extracted Δ_{asym} values for the transitions of ^{77}As are depicted in Fig. 2.

TABLE I. Initial level energies E_x^i in keV, gamma transition energies E_γ in keV, relative intensities (RI), initial (J_i^π), and final (J_f^π) spins, DCO ratios (R_{DCO}), polarization asymmetries ($\Delta_{\rm asym}$), and assigned multipolarities for the observed transitions belonging to ^{77}As. The newly observed levels and γ transitions are highlighted with bold faces. The level energies have been obtained by making least square fit to the corresponding γ transition energies using the code GTOL [48].

E_x^i (keV)	E_γ (keV)	RI	$J_i^\pi \rightarrow J_f^\pi$	R_{DCO}	$\Delta_{\rm asym}$	Multipolarity
215.64(10)	215.7(1)	14.1(20)	$3/2^- \rightarrow 3/2^-$	0.92(5)[a]	0.19(11)	$M1+E2$
264.51(10)	264.5(1)		$5/2^- \rightarrow 3/2^-$	0.53(3)[b]	−0.05(6)	$M1+E2$
475.71(14)	211.2(1)		$9/2^+ \rightarrow 5/2^-$	0.95(2)[c]	0.01(3)	$M2+E3$
631.99(13)	367.5(2)	3.1(2)	$5/2^+ \rightarrow 5/2^-$	1.46(8)[c]	−0.03(6)	$E1$
	416.5(2)	4.8(3)	$\rightarrow 3/2^-$	1.05(10)[d]	0.07(6)	$E1$
	631.8(4)	1.6(3)	$\rightarrow 3/2^-$	1.03(10)[d]		$(E1)$
784.9(4)	520.4(4)	1.5(1)	$7/2^- \rightarrow 5/2^-$	1.01(10)[c]		$(M1+E2)$
889.18(23)	624.5(4)	1.7(1)	$5/2 \rightarrow 5/2^-$	1.62(11)[c]		$D(+Q)$
	673.7(4)	1.2(1)	$\rightarrow 3/2^-$			$[D+Q]$
1048.70(17)	573.0(1)	100(4)	$13/2^+ \rightarrow 9/2^+$	0.99(3)[e]	0.17(6)	$E2$
1058.92(14)	794.4(1)	12(1)	$9/2^- \rightarrow 5/2^-$	2.09(8)[c]	0.05(4)	$E2$
1190.25(23)	558.3(2)	8(1)	$7/2^- \rightarrow 5/2^+$	0.89(6)[a]	0.09(6)	$E1+M2$
1221.47(17)	745.7(1)	36.4(30)	$11/2^+ \rightarrow 9/2^+$	0.88(6)[i]	−0.02(3)	$M1+4\%\,E2$
1345.4(5)	1080.9(4)	1.4(1)	$(7/2) \rightarrow 5/2^-$	0.91(10)[c]		$D(+Q)$
1399.0(3)	208.8(4)	1.3(1)	$(9/2^+) \rightarrow 7/2^-$	0.87(10)[d]		$(E1)$
	766.8(4)	1.0(1)	$\rightarrow 5/2^+$	1.65(18)[c]		$(E2)$
1457.8(4)	1193.3(4)	1.6(2)	$(5/2,7/2) \rightarrow 5/2^-$	1.33(15)[c]		$D(+Q)$
1526.1(5)	1261.6(5)	0.6(1)	$\rightarrow 5/2^-$			
1737.03(18)	515.5(1)	20.3(20)	$13/2^+ \rightarrow 11/2^+$	0.93(6)[k]	−0.06(4)	$M1+1\%\,E2$
	687.9(5)[o]	0.8(1)	$\rightarrow 13/2^+$			$[M1+E2]$
	1261.6(5)[o]	Weak	$\rightarrow 9/2^+$			$[E2]$
1888.71(18)	840.0(1)	27.9(34)	$15/2^+ \rightarrow 13/2^+$	0.48(3)[h]	−0.009(28)	$M1+14\%\,E2$
	667.0(4)	1.4(2)	$\rightarrow 11/2^+$	1.49(13)[g]		$(E2)$
1901.2(6)[o]	**1012.0(5)**[o]	0.5(1)	$\rightarrow 5/2$			
2000.58(19)	951.9(1)	32.7(20)	$17/2^+ \rightarrow 13/2^+$	0.96(5)[h]	0.10(4)	$E2$
2123.72(25)	1064.8(2)	4.4(4)	$13/2^- \rightarrow 9/2^-$	2.23(15)[c]	0.08(6)	$E2$
2289.1(5)	**400.4(5)**	0.8(1)	$(17/2) \rightarrow 15/2^+$	0.69(9)[h]		$D(+Q)$
2513.12(20)	624.4(2)	6.2(5)	$17/2^+ \rightarrow 15/2^+$	0.50(4)[h]	−0.012(55)	$M1+14\%\,E2$
	776.1(4)	2.3(4)	$\rightarrow 13/2^+$	1.65(12)[f]		$(E2)$
	1464.4(4)	1.4(2)	$\rightarrow 13/2^+$	1.02(15)[h]		$(E2)$
2584.72(23)	1363.4(2)	5.1(5)	$13/2^- \rightarrow 11/2^+$	1.21(10)[j]	0.09(7)	$E1$
2745.67(21)	161.1(2)	4.1(4)	$15/2^- \rightarrow 13/2^-$	0.96(5)[j]		$(M1+E2)$
	1008.5(2)	5.4(4)	$\rightarrow 13/2^+$	0.97(5)[f]	0.07(6)	$E1$
	1697.0(4)	2.9(3)	$\rightarrow 13/2^+$	0.59(10)[h]	0.11(11)	$E1$
2881.89(24)	881.3(2)	6.0(4)	$19/2^+ \rightarrow 17/2^+$	0.48(4)[h]	0.017(73)	$M1+20\%\,E2$
	993.0(4)	2.5(4)	$\rightarrow 15/2^+$	1.07(9)[h]	0.09(9)[n]	$E2$
3003.6(3)	258.0(2)	8.8(5)	$17/2^- \rightarrow 15/2^-$	0.62(6)[h]	−0.04(7)	$M1+E2$
	1114.7(5)	0.9(2)	$\rightarrow 15/2^+$	1.03(15)[k,n]		$(E1)$
3150.9(3)	1150.4(1)	11.2(10)	$21/2^+ \rightarrow 17/2^+$	1.03(5)[e]	0.07(5)	$E2$
3290.2(4)	**1166.5(4)**	1.3(2)	$17/2^{(-)} \rightarrow 13/2^-$	1.52(15)[c]		$(E2)$
3364.9(4)	361.3(2)	7.8(5)	$19/2^- \rightarrow 17/2^-$	1.04(4)[j]	−0.08(6)	$M1+E2$
3568.2(4)	**1055.0(4)**	1.1(2)	$(21/2^+) \rightarrow 17/2^+$			$[E2]$
	1567.6(5)	0.7(2)	$\rightarrow 17/2^+$			$[E2]$
3732.4(6)	**1443.3(4)**	1.2(2)	$(19/2) \rightarrow (17/2)$	0.76(9)[h,n]		$(D+Q)$
3857.1(4)	492.2(2)	5.0(3)	$21/2^- \rightarrow 19/2^-$	1.04(6)[k]	−0.06(4)	$M1+E2$
4051.8(4)	**901.1(4)**	1.6(2)	$(23/2^+) \rightarrow 21/2^+$	0.45(10)[l,n]		$(M1+E2)$
	1169.6(5)	0.9(2)	$\rightarrow 19/2^+$			$[E2]$
4455.5(4)	1304.6(2)	3.9(4)	$25/2^+ \rightarrow 21/2^+$	1.14(12)[l]	0.07(11)	$E2$
4476.6(5)	**619.5(4)**	1.7(2)	$23/2^{(-)} \rightarrow 21/2^-$	0.95(10)[j]	−0.09(9)[n]	$M1+E2$
4753.2(7)[o]	**1185.0(5)**[o]	Weak	$(25/2^+) \rightarrow (21/2^+)$			$[E2]$
5152.4(7)	**675.8(5)**	0.8(1)	$(25/2^-) \rightarrow 23/2^{(-)}$	0.97(13)[m,n]		$(M1+E2)$

TABLE I. (*Continued.*)

E_x^i (keV)	E_γ (keV)	*RI*	$J_i^\pi \rightarrow J_f^\pi$	R_{DCO}	Δ_{asym}	Multipolarity
5903.5(7)	**1448.0(5)**	0.7(2)	$(29/2^+) \rightarrow 25/2^+$			[*E*2]
7499.0(9)[o]	**1595.4(5)**[o]	Weak	$(33/2^+) \rightarrow (29/2^+)$			[*E*2]

[a]Deduced using the 416 keV, *E*1 gate.
[b]Deduced using the 794 keV, *E*2 gate.
[c]Deduced using the 264 keV, $M1 + E2$ gate.
[d]Deduced using the 558 keV, $E1 + M2$ gate.
[e]Deduced using the 952 keV, *E*2 gate.
[f]Deduced using the 515 keV, $M1 + E2$ gate.
[g]Deduced using the 746 keV, $M1 + E2$ gate.
[h]Deduced using the 573 keV, *E*2 gate.
[i]Deduced using the 1008 keV, *E*1 gate.
[j]Deduced using the 258 keV, $M1 + E2$ gate.
[k]Deduced using the 361 keV, $M1 + E2$ gate.
[l]Deduced using the 1150 keV, *E*2 gate.
[m]Deduced using the 492 keV, $M1 + E2$ gate.
[n]The DCO-ratio and polarization value could not be extracted unambiguously due to the presence of close-lying doublet transition.
[o]Tentatively placed in the level scheme.

III. EXPERIMENTAL RESULTS

The proposed level scheme of ^{77}As as obtained from the present $\gamma\gamma$ coincidence analysis is shown in Fig. 3. A total of nineteen new transitions and twelve new levels have been added to the existing level scheme. This leads to the extension of the level scheme up to $E_x \approx 7.5$ MeV and $J = 33/2\,\hbar$. The newly observed transitions have been marked with $*$ in the level scheme presented in Fig. 3. As can be seen from the figure, the sequence of levels have been categorized under five different groups for the sake of convenience in bringing out the fruitful discussion. The spectroscopic results obtained from the present experiment are summarized in Table I. The quoted uncertainties associated with the R_{DCO}, and Δ_{asym} values are statistical only. The uncertainties for the relative intensities of the γ rays are quoted by adding in quadrature a 5% uncertainty due to efficiency correction to the associated statistical uncertainties. The uncertainties are considered to be 0.1, 0.2, 0.4, and 0.5 keV for the energies of the γ transitions having relative intensities $RI > 10$, >3, >1, and <1, respectively. The necessary discussion related to the positive- and negative-parity level sequences has been provided one by one in the following subsections.

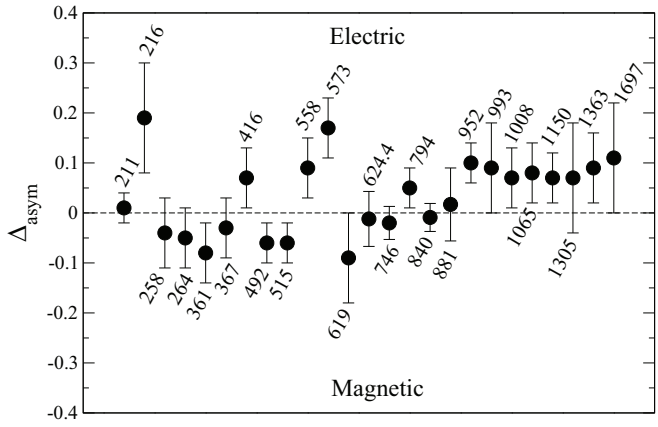

FIG. 2. The experimental asymmetry (Δ_{asym}) values for the transitions of ^{77}As obtained from the polarization measurement. The dotted line through the zero value of asymmetry has been drawn to guide the eye.

A. Positive-parity levels

The yrast positive-parity band, built upon the isomeric $9/2^+$ state ($T_{1/2} = 116\ \mu$s), was previously known up to $E_x = 4455$ keV and $J^\pi = 25/2^+$. In the present work, the band has been extended up to $E_x = 7499$ keV and $J^\pi = (33/2)^+$ by placing two new transitions having energies 1448 and 1595 keV that feed the $25/2^+$, 4455 keV, and $(29/2)^+$, 5903 keV levels, respectively (see Fig. 3).

A representative $\gamma\gamma$ coincidence spectra corresponding to the gates of 573-, and 1305-keV transitions, belonging to band-1a, are shown in Figs. 4(a) and 4(b), respectively. The inset Fig. 4(c) provides the spectrum gated by the interband (1b $\rightarrow$ 1a) 881-keV transition of ^{77}As. The placements of the new γ transitions, 1448- and 1595-keV of band-1a are justified from the coincidence spectra of Figs. 4(a) and 4(b). It is worthwhile mentioning that the previously reported *E*2 multipolarities of the known transitions of band-1a up to the $25/2^+$, 4455 keV [4] state got confirmed from the present investigation following the extracted values of angular asymmetry (R_{DCO}) in conjunction to the polarization asymmetry (Δ_{asym}). As the 1448- and 1595-keV transitions of band-1a are very weak in intensities, no DCO and polarization measurements could be made possible for those transitions. However, based on the observed regularity, *E*2 multipolarities have been assigned tentatively for the 1448- and 1595-keV transitions. The previously reported 1221- and 1889-keV levels along with the newly observed 2882- and 4052-keV levels

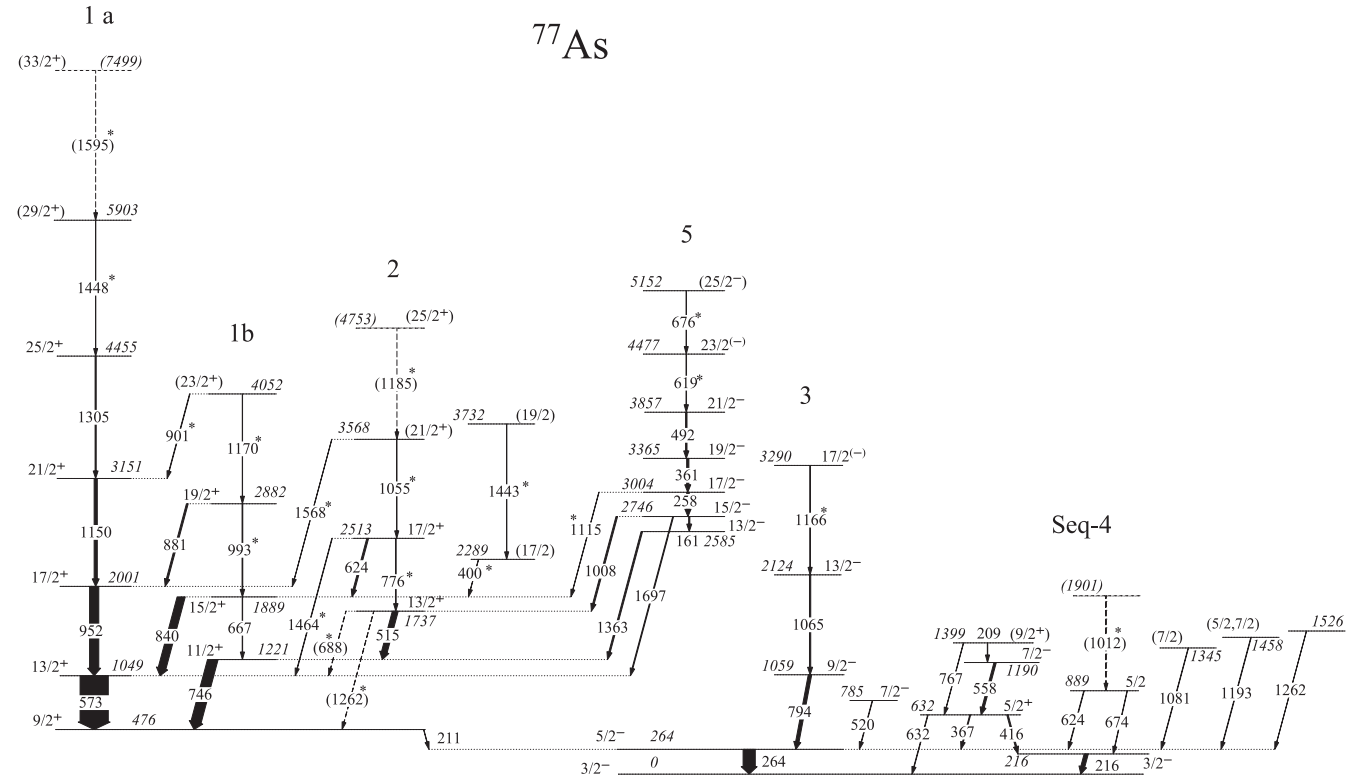

FIG. 3. Proposed level scheme of ^{77}As as deduced from the present investigation. The newly observed γ rays have been marked with $*$. The level and γ-ray energies are given in keV. The widths of the arrows are proportional to the relative intensities of the transitions. The dotted arrow-lines represent tentatively placed γ rays. The tentative levels are marked with the dotted horizontal lines.

are proposed to form the unfavored signature ($\alpha = -1/2$) band (band-1b of Fig. 3). It should be mentioned here that Doring *et al.* [4] considered 1221- and 1889-keV states to be the possible candidature for the signature partner band of the yrast positive-parity band built on the $9/2^+$ state. The placements of the newly observed 993- and 1170-keV intraband γ transitions of band-1b can be justified from the coincidence spectra of Figs. 4(c) and 5(a). Band-1b is found to decay to band-1a via the 746-, 840-, 881-, and 901-keV interband transitions. Figure 4(a) demonstrates the conformity of the placements of the said transitions. In the previous investigation of Ref. [4], a level at 1930 keV was placed based on the

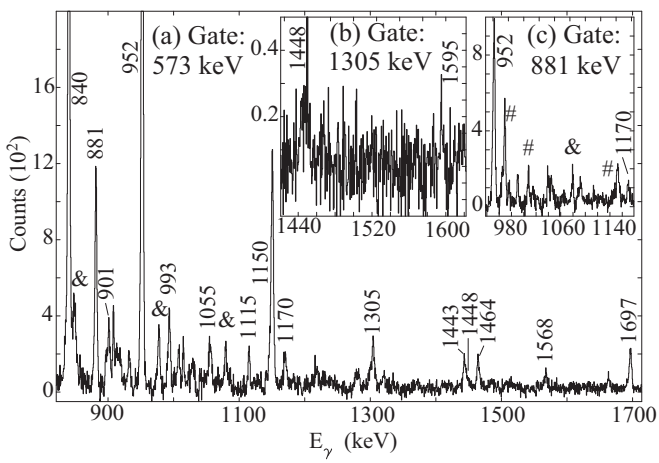

FIG. 4. Representative $\gamma\gamma$ coincidence spectra with the energy gates set on (a) 573-keV, (b) 1305-keV, and (c) 881-keV transitions of ^{77}As. The peaks assigned to ^{77}As are marked by their energies in keV. The identified contaminant peaks have been marked as # and & and belong to ^{78}Se and ^{77}Se, respectively.

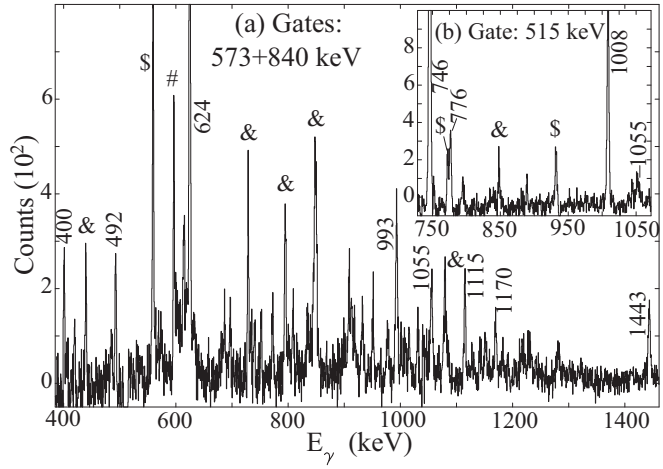

FIG. 5. Partial $\gamma\gamma$ coincidence spectra obtained by gating on (a) 573 + 840-keV and (b) 515-keV transitions of ^{77}As. Peaks labeled with their energy values (in keV) have been assigned to ^{77}As. The contaminant peaks arising from ^{77}Se, ^{74}Ge, and ^{76}Se are indicated with &, #, and $, respectively.

709- and 881-keV transitions feeding the 1221- and 1049-keV levels, respectively. Based on the present coincidence analysis, the 881-keV transition has been placed from 2882-keV level. The present analysis does not provide any evidence for the presence of the 709-keV transition and hence, not being placed in the level scheme (see Fig. 3). Hence, the 1930 keV level has been removed from the present level scheme. The extracted DCO and polarization asymmetry values for the 881- and 993-keV transitions lead to a firm assignment of $19/2^+$ for the 2882-keV level. A tentative assignment of $(23/2^+)$ has been made for the 4052-keV level as the DCO ratio of the 901-keV transition decaying from the level could not be measured unambiguously.

The sequence comprising of the previously reported levels at 1737- and 2513- keV along with the newly observed levels at 3568- and 4753-keV are proposed to form band-2 (see Fig. 3). It is found that the levels of band-2 preferentially decay to band-1b; whereas the comparatively weaker decay branches from band-2 feed the levels belonging to band-1a. The 1737- and 2513-keV levels are found to decay to the 1221- and 1889-keV levels of band-1b via the intense 515- and 624-keV γ transitions, respectively. The measured Δ_{asym} and R_{DCO} values for the 515- and 624-keV transitions provide an unambiguous spin-parity assignments of $13/2^+$ and $17/2^+$ for the 1737- and 2513-keV levels, respectively. The coincidence spectrum of 1055-keV transition provides the indication for the presence of 1185-keV transition decaying from the 4753-keV level. However, the 1185-keV transition has been tentatively placed in the decay scheme due to the lack of sufficient coincidence statistics. The placements of the newly observed intraband γ rays belonging to band-2 as well as the other γ rays that decay from band-2 and feed the yrast level sequences of bands-1a and 1b are found to be got confirmed from the coincidence spectra of Fig. 5(b), Fig. 5(a), and Fig. 4(a), respectively. It is interesting to note that a similar kind of sequence of levels was also observed previously in the isotone ^{79}Br [1].

It can be seen from Fig. 1 that the extracted DCO values of the interband linking 515-, 624-, 746-, 840-, and 881-keV transitions with $M1 + E2$ multipolarities are found to be somewhat less than the expected value corresponding to the depicted $\Delta J = 1$ line. Following this observation, an attempt has been made to determine the associated mixing ratio values (subsequently the percentage estimation of $E2$ component) for the concerned transitions with the help of the ANGCOR code [22] and using the analysis procedure as described in Ref. [24]. The extracted mixing ratio values indicate that the transitions are predominantly $M1$ in nature (see Table I).

B. Negative-parity levels

The negative-parity band (band-5) built on the $13/2^{(-)}$, 2585 keV level was previously reported in Ref. [4] up to the excitation of $E_{ex} = 3857$ keV with the placements of the 161-, 258-, 361-, 492-keV γ rays decaying from 2746-, 3004-, 3365-, and 3857-keV levels, respectively. In the present investigation, all those previously reported γ rays have been observed. Furthermore, the present investigation has made it possible to extend the band up to an excitation of 5152-keV

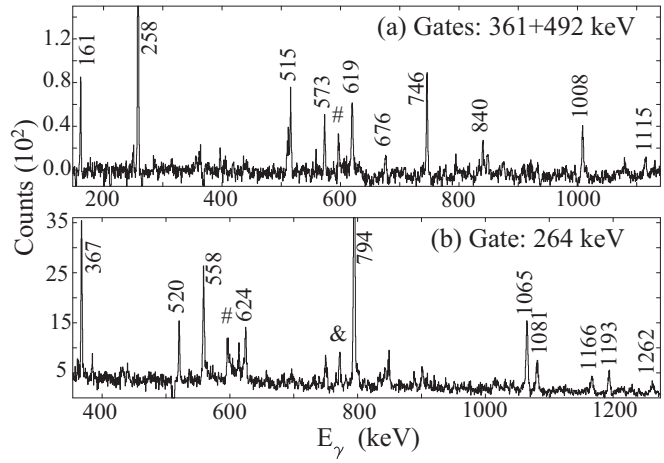

FIG. 6. Representative $\gamma\gamma$ coincidence spectra with the energy gates set on (a) 361- and 492- (b) 264-keV transitions of ^{77}As. Only the peaks assigned to ^{77}As are marked by their energies (in keV). The contaminant peaks identified with # and & belong to ^{74}Ge and ^{77}Se, respectively.

by placing two new transitions of 619-, and 676-keV that feed the $21/2^-$, 3857-keV and $23/2^{(-)}$, 4477-keV levels, respectively. The 1115-keV decay branch from the 3004-keV level of band-5 has newly been placed in the decay scheme. It is to be noted here that no γ rays from band-5 have been found to decay to the negative-parity level sequences of band-3. This feature seems to differ somewhat in comparison to the decay sequences observed in the neighboring isotopes [7] and isotones [1]. All the intraband transitions of band-5, and the interconnecting transitions to the positive-parity levels of bands-1a, 1b, and 2 can be seen in the coincidence spectrum shown in Fig. 6(a). The parity of the bandhead of band-5 was assigned tentatively in the previous work of Ref. [4]. In the present work, a firm spin-parity assignment of $13/2^-$ has been made for the bandhead on the basis of the positive value of polarization asymmetry measured for the 1363-keV transition. Also, the magnetic nature for the cascading 258-, 361-, 492-keV transitions have been ascertained based on the extracted polarization asymmetry values. However, due to weak intensities, unambiguous polarization measurements could not be made possible for the other cascading transitions decaying from the levels lying above 3857-keV excitation. No crossover $E2$ transitions have been identified in the observed dipole band, band-5.

The previously reported [4] negative-parity ground state band (band-3) has been extended up to 3290-keV excitation energy by newly adding the 1166-keV transition. The extracted DCO- and polarization asymmetry values (see Table I) for the 1065-keV γ ray suggest for a stretched $E2$ character. The extracted DCO value is found to be consistent with that for the 794-keV transition having the known $E2$ character.

Attempt has also been made to undertake the multipolarity measurements of a few of the transitions belonging to the highly irregular level sequences (see the group of levels under Seq-4 of Fig. 3). The spin-parity assignments for majority of the levels were tentative in the previous work [4]. The

spin-parity assignment for the 1399-keV level has been made as $(9/2^+)$ in the present investigation. A $(7/2^+)$ assignment was previously made for the 1399-keV level. The tentatively reported $5/2^{(+)}$ assignment [4] for the 632 keV level also gets confirmed from the present polarization measurements of the two intense 367- and 416-keV depopulating transitions. The 1012-keV transition has been placed tentatively based on the coincidence relation with the 264 keV gate. The cascading transitions those belong to Seq-4 and are in coincidence with the ground state feeding 264-keV transition can clearly be seen in the coincidence spectrum of Fig. 6(b).

IV. DISCUSSION

The observed excited levels of ^{77}As have been classified under six different groups (see Fig. 3) for the sake of convenience in bringing out the necessary discussion. For proper interpretation of the nuclear level structure issues associated with the different bands of ^{77}As, the necessary theoretical calculations have been carried out within the framework of total Routhian surface (TRS), shell model (SM), particle plus triaxial rotor model (TPRM), and semiclassical treatment. The underlying features unveiled for the different bands are discussed in the following subsections.

A. Yrast positive-parity states (bands-1a and 1b)

The yrast positive-parity band built on the isomeric $9/2^+$, 476-keV level was known up to the excitation of $E_{ex} = 4455$ keV with $J^\pi = 25/2^+$ from the previous work of Döring *et al.* [4]. The yrast positive-parity states were attributed to the proton excitations involving the $\pi(g_{9/2})$ orbital [4]. However, the level structure was not extended to the crossing frequency regime.

Following the extended level scheme as deduced from the present work, the kinematic moment of inertia ($J^{(1)}$), dynamic moment of inertia ($J^{(2)}$), and aligned angular momentum (i_x) have been determined for band-1a at different rotational frequencies ($\hbar\omega$), and the variations have been shown in Fig. 7. The values of the Harris parameters used for calculating the reference rotor angular momentum are the same as that utilized in the case of TPRM calculations. Figure 7(a) shows that the rising pattern curve in $J^{(1)}$ (kinematic moment of inertia) for ^{77}As has a slight difference than that for the nearest isotone, ^{79}Br in the rotation frequency regime above $\hbar\omega \approx 0.6$ MeV. However, both the curves approach each other at about $\hbar\omega \approx 0.8$ MeV. Such kind of features can also be clearly seen in the alignment plots of Fig. 7(c). Figure 7(b) demonstrates the variation profile of the dynamic moment of inertia, $J^{(2)}$ for ^{77}As and ^{79}Br. The figure clearly indicates a large enhancement for ^{79}Br at $\hbar\omega \approx 0.60$ MeV, whereas such a large enhancement is not seen for ^{77}As at the corresponding band crossing regime of $\hbar\omega \approx 0.65$ MeV. As pointed out in Ref. [3], such a large enhancement in the $J^{(2)}$ value was also found (not shown in Fig. 7) for the neighboring ^{73}As isotope at $\hbar\omega \approx 0.50$ MeV corresponding to the first band crossing regime. The large enhancement in $J^{(2)}$ value for ^{73}As and ^{79}Br have been interpreted as due to the presence of relatively weaker interaction strength associated with the pair of $\nu(g_{9/2})$

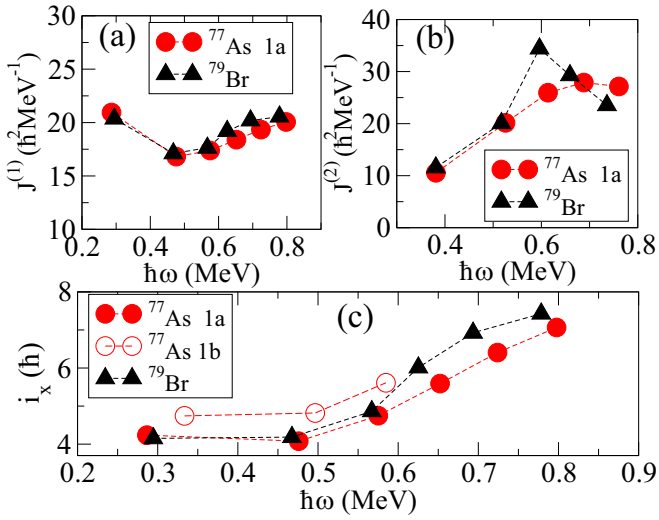

FIG. 7. The variation of (a) kinematic moment of inertia $J^{(1)}$, (b) dynamic moment of inertia $J^{(2)}$, and (c) neutron alignments as a function of rotational frequency, $\hbar\omega$ for the yrast positive-parity states of ^{77}As and ^{79}Br. The data for ^{79}Br are taken from [1].

alignment for generating the band-crossing phenomena [1,3]. The relatively smaller gain in $J^{(2)}$ value for ^{77}As is possibly due to the involvement of moderate interaction strength for the $\nu(g^2_{9/2})$ alignment that leads to the crossing of bands above the 4455-keV, $25/2^+$ state. After the occurrence of first band crossing at $\hbar\omega \approx 0.65$ MeV, the single quasiparticle $\pi(g_{9/2})$ band structure is considered to change to a three quasiparticle $\pi(g_{9/2})\ \nu(g_{9/2})^2$ band structure similar to what has been reported for ^{73}As in Ref. [3].

The nature of the quasiparticle alignment and the possible shape change phenomena due to the effect of first band crossing has been further investigated by the total Routhian surface (TRS) calculation. The calculations are based on the Hartree-Fock-Bogolyubov formalism as described in Refs. [25,26]. The calculations have been performed at the rotational frequencies of $\hbar\omega = 0.30$ and 0.65 MeV that simulates the situation prior to and at the vicinity of the first band crossing regime, respectively. The calculation predicts a triaxial shape with $\beta_2 \approx 0.29$ and $\gamma \approx 31^\circ$ at $\hbar\omega = 0.30$ MeV. At the vicinity of band-crossing regime of $\hbar\omega = 0.65$ MeV, the calculated result suggest for a shape featured with the deformation parameter values of $\beta_2 \approx 0.25$, and $\gamma \approx -38^\circ$. Thus, the triaxial shape seems to persist in the positive-parity yrast band structure of ^{77}As spanning the regime of lower-frequency to that of the first-band crossing. However, the change in the sign of γ parameter indicates the onset of nonrigid triaxial feature for the associated band structure.

B. Particle plus triaxial rotor model calculations

The particle plus triaxial-rotor model (TPRM) is a powerful tool to study the microscopic structure of a rotational band. Under this framework, the effect of γ deformation on the signature splitting of a rotational band can be addressed in a proper way [27,28]. To understand the underlying mechanism for the development of the bands-1(a,b) of ^{77}As, TPRM

calculations have also been carried out in the present work. As per the prescription of TPRM, the particle-rotor Hamiltonian of an odd-A nucleus is expressed as

$$H = H_{\text{core}} + H_{sp} + H_{\text{pair}},$$

where H_{core} represents the collective rotation of the even-even core and can be written as

$$H_{\text{core}} = \sum_{k=1}^{3} A_k (I_k - j_k)^2.$$

The parameters A_k represent the inertial parameters. The moments of inertia are assumed to be of hydrodynamical type and depend on the deformation. In the present set of calculations, the variable moment of inertia (VMI) formalism [29] has been used for estimating the level energies of the core nucleus ^{76}Ge. The Harris parameters [30], $\mathrm{I_0} = 9.09\hbar^2$ MeV^{-1} and $\mathrm{I_1} = 5.26\hbar^4$ MeV^{-3}, have been used to derive the VMI parameters, A00 and STIFF. The single-particle Hamiltonian H_{sp} is governed by the deformation parameters ϵ and γ. The necessary quasiparticle energies for the concerned particle-plus-rotor system have been calculated following the modified oscillator (Nilsson) potential with the standard set of κ and μ parameters [31]. The pairing interaction has been incorporated by the term H_{pair} and estimated via the standard BCS procedure. Detailed formalism of the model can be found in Refs. [32,33]. In the calculation, the core nucleus (^{76}Ge) has been considered to be axially asymmetric. The rigid triaxial nature of ^{76}Ge has firmly been established in the recent works of Ayangeakaa *et al.* [34,35]. The present formalism deals with the motion of the unpaired odd-proton that moves in the Nilsson's deformed orbital and couples to the rotational motion of the core through Coriolis interaction.

Figure 8 shows a comparison of the calculated level energies with the experimental level energies of band-1. The calculations have been carried out with the values of the deformation parameters, $\epsilon_2 = 0.25$ and $\gamma = 25^\circ$ and a good agreement between the experimental and theoretical level energies is obtained. The experimental level energies are found to be reproduced well after allowing the admixture of $\pi d_{5/2}$ and $\pi g_{9/2}$ states for describing the motion of the odd-particle. This is similar to what has been reported previously for the lighter odd-mass ^{71,73}As isotopes [36]. The occupancy of the odd-particle in both the 1/2[440] and 3/2[431] orbitals seem to significantly contribute in generating the underlying wave functions of the states.

In Fig. 9, the experimentally observed staggering pattern for the bands-1(a,b) has been compared with the corresponding calculated results following TPRM calculations. Here, the staggering parameter $S(I)$ has been extracted using the relation, $S(I) = [E(I) - E(I-1)]/2I$, where $E(I)$ is the energy of the state with spin I. Based on the consideration of hydrodynamical moment of inertia in the present TPRM calculation, the intermediate axis should be the preferred axis for the collective rotation of the triaxial core [37]. Under this scenario, the signature quantum number becomes approximately a good quantum number only when the single particle angular momentum of the valence odd particle aligns along the intermediate axis. Figure 9 brings out the fact that the experimental pattern of staggering is well reproduced for the lower spin states. The good agreement between the observed and calculated $S(I)$ values at the regime of lower spins suggests for the alignment of the angular momentum associated with the $\pi(g_{9/2})$ orbital along the intermediate axis. To explore the aforesaid issue quantitatively, the angular-momentum expectation value $\langle \vec{R} \cdot \vec{j}_\pi \rangle / \mid R \mid$ [38] has been calculated using

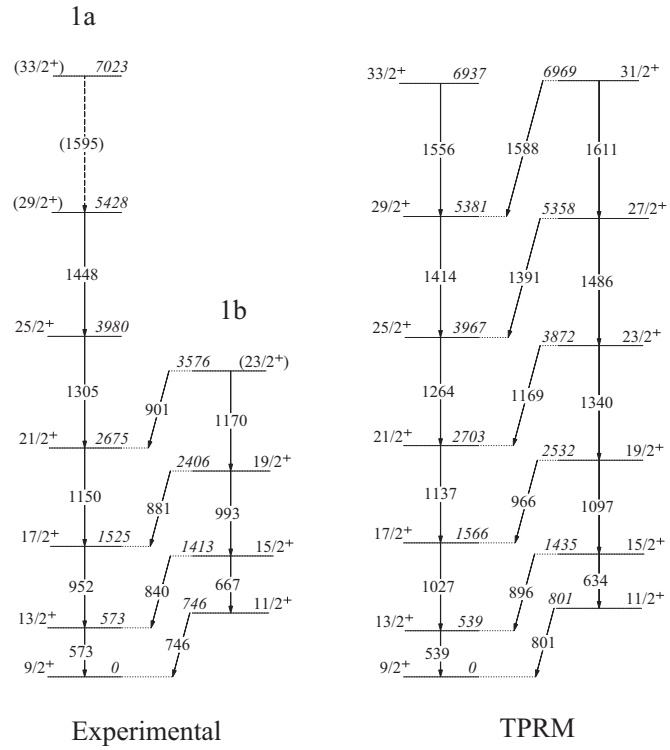

FIG. 8. Comparison of the experimentally observed energies of the levels belonging to bands-1(a,b) with the corresponding level energies predicted from TPRM calculation.

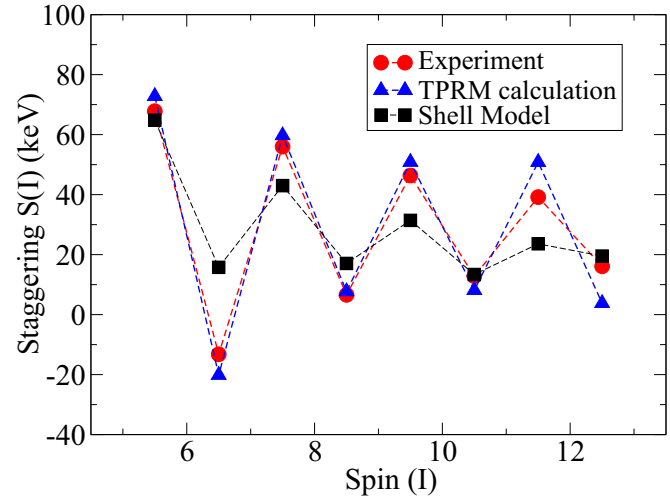

FIG. 9. Comparison between the experimentally observed and theoretically predicted staggering patterns associated with the signature partner bands, 1(a,b) of ^{77}As.

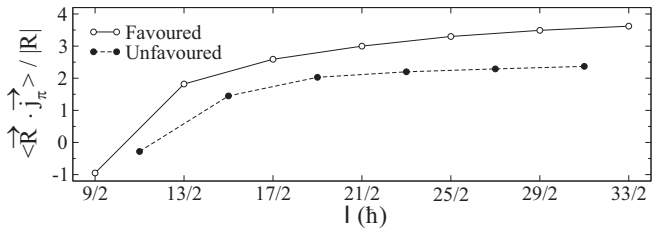

FIG. 10. The variation in the expectation value, $\langle \vec{R} \cdot \vec{j}_\pi \rangle / \mid R \mid$ as a function of angular momentum, I for the $\pi g_{9/2}$ band in ^{77}As.

the TPRM wave function. The quantity related to the expectation value represents the alignment (i.e., projection) of the unpaired quasiproton angular momentum (j_π) in the direction of the collective rotation vector R. As shown in Fig. 10, the calculated expectation value is found to be negative at the lowest spin, thereby indicating an anti-alignment of $\vec{R}$ and $\vec{j}_\pi$ near the bandhead. However, the odd-quasiproton starts aligning with the collective rotation with increasing spin, and as a consequence a sudden jump in the expectation value has been observed (see Fig. 10). The alignment process is found to be quite similar for both the sequences, 1a and 1b. These subsequently lead to the approximate validation of the 1b band as the signature partner of the 1a band, built on the $\pi(g_{9/2})$ configuration, of ^{77}As. The similar pattern of variation of aligned angular momenta i_x for the bands-1(a,b) [see Fig. 7(c)] also indicates their signature partner behavior [39]. Figure 9 shows the deviations between the experimental and theoretical values of $S(I)$ for the higher-spin states of bands-1(a,b). This is possibly due to the gamma-soft nature of ^{77}As as predicted from the TRS calculations. The experimentally observed staggering pattern has also been compared in Fig. 9 to that of the predicted pattern from the shell-model calculations as prescribed in the following section. A reasonable reproduction of the overall experimental profile of staggering can be seen from the figure.

C. Shell-model calculations

To understand the dominant configurations of the experimentally observed levels in ^{77}As, the large-scale shell-model (SM) calculations have been performed using two different sets of effective interactions, JUN45 and jj44b [40]. The calculations were carried out using the code NUSHELLX [41]. The jj44 model space comprising the π, $\nu(2p_{3/2}, 1f_{5/2}, 2p_{1/2}, 1g_{9/2})$ valance orbitals outside the ^{56}Ni core have been used for the calculations. The comparison between the experimentally observed and theoretically predicted level energies is made in Fig. 11. The figure includes only those observed levels for which the definitive or tentative spin-parity assignments could be made in the present investigation.

As can be seen from Fig. 11(a), both the JUN45 and jj44b interactions predict correctly the $3/2^-$ ground-state spin. Also, except for a few cases, the orderings of the experimentally observed negative-parity levels (belonging to Seq-4, bands-3 and 5) with $E_{ex} > 700$ keV are reproduced well in both sets of calculations. The mean level deviation (MLD) values between the experimentally observed and theoretically predicted negative-parity levels are found to be 108 and 258 keV for JUN45 and jj44b, respectively. This brings out the fact that JUN45, on the average, provide better predictions for the negative-parity levels in comparison to that following jj44b calculations.

The comparison between the experimental and calculated results for the positive-parity energy levels are also shown in Fig. 11(b). The figure indicates that both the JUN45 and jj44b

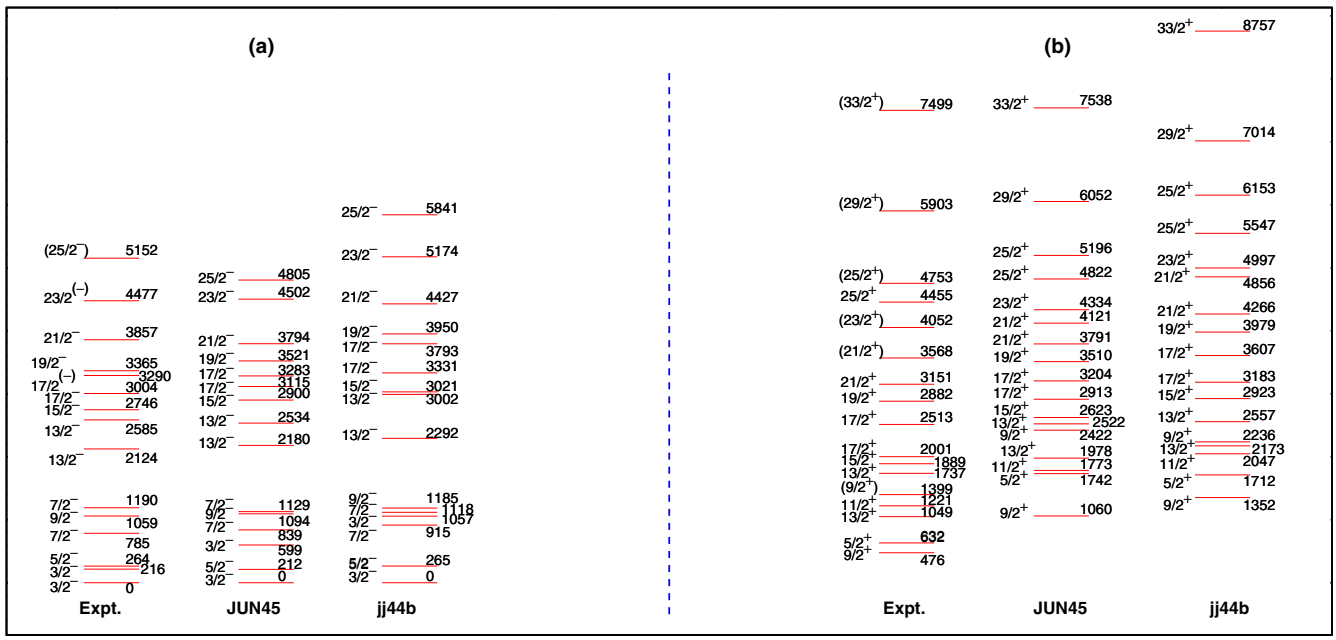

FIG. 11. Comparison of the experimentally observed levels of ^{77}As with those of the predicted levels from the shell-model calculations using JUN45 and jj44b interactions.

interactions predict $9/2^+$ as the spin-parity for the lowermost positive-parity level. However, the calculated level energy is found to be higher than the corresponding experimental level energy by more than 500 keV in both the calculations. Both the interactions predict that the energy of the first excited $13/2_1^+$ state is higher than that of the first-excited $11/2_1^+$ state. But the reverse ordering has been observed from the experimental findings. Except these, the orderings of all the other experimentally observed levels belonging to the band structure of 1a, 1b, and 2 are found to be correctly reproduced in both the calculations. The mean level deviation (MLD) values between the experimentally observed and theoretically predicted positive-parity levels are found to be 625 and 771 keV for JUN45 and jj44b, respectively. Hence, as in the case of negative-parity levels, overall better predictions can be seen for JUN45 in comparison to those for jj44b. It is important to note that the predicted results of the higher-lying energy levels following JUN45 calculation also corroborates the $J^\pi = (29/2^+)$, $(33/2^+)$ assignments for the experimentally observed 5903- and 7499- keV levels, respectively. The extracted MLD values point towards the fact that the negative-parity levels are on an average better reproduced in comparison to that of the positive-parity levels by both the interactions.

As the overall predicted level energies from JUN45 calculations seem to provide comparatively better agreement with the experimental results in comparison to that from jj44b calculations, a brief discussion on the results obtained from the JUN45 calculations has been put forward. The calculations suggest $\pi(p_{3/2})^3$ as the dominating partition for the underlying wave functions of the observed $3/2^-$ ground-state level. The observed $9/2^+$, 476 keV bandhead of the yrast positive-parity band is found to originate mainly from the $\pi(g_{9/2})^1$ configuration. The calculated occupation probabilities also point to the fact that the shape driving $1g_{9/2}$ proton orbital has no role in generating the negative-parity states belonging to band-3. This leads to the onset of less deformation in the observed band structure. This is reflected in the larger separation in energies between the bandhead and the first-excited state.

D. Nonyrast positive-parity band (band-2)

The observed decay patterns of the levels of band-2 of ^{77}As are found to be quite similar with those of the band members belonging to the γ band of ^{76}Ge (see band-3 of Ref. [42]). It is to be pointed out here that the population strength for the bandhead of band-2 is found to be about two times weaker than that of the bandhead of the yrast $\alpha = -1/2$ positive-parity band. This seems to be the reason for the nonobservance of the corresponding partner band members (members with $J^\pi = 15/2^+$, $19/2^+$, and $23/2^+$) in the present investigation. The experimentally observed level energies of band-2 are compared with the calculated level energies in Fig. 12. The calculated levels are obtained by adding the bandhead energy and spin of band-1 to the corresponding even-spin levels of gamma band of ^{76}Ge. As can be seen from the figure, except for the bandhead energy, the energies of the other levels of band-2 are nicely reproduced. The band-2 thus can be considered to be a quasi-γ band [43] originating from the coupling between the odd $g_{9/2}$ quasiproton and the γ vibration of the core nucleus ^{76}Ge.

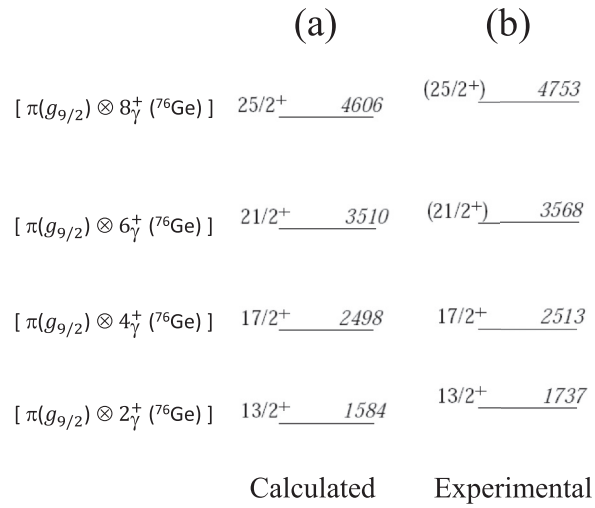

FIG. 12. Comparison between the experimental and calculated energies of the levels belonging to band-2 of ^{77}As. The calculated level energies are obtained from the coupling of the $\pi(g_{9/2})$ bandhead of band-1 with the corresponding members of the γ-vibration band of the core nucleus ^{76}Ge (see text for details).

E. High-lying negative-parity band (band-5)

The presence of high-lying negative-parity bands with the dominance of $\Delta I = 1$ transitions were previously observed in the neighboring isotope, ^{75}As [7] and the isotone, ^{79}Br [1]. The experimental results point to the fact that the levels belonging to these bands decay predominantly through $M1$ transitions with the associated large $B(M1)$ values [1]. The previously reported negative-parity band of ^{77}As was found to be built on the $13/2^-$, 2585 keV bandhead and interpreted in terms of the 3qp $\pi[(g_{9/2})] \otimes \nu[(g_{9/2})(fp)]$ configuration [4]. Unlike to the cases for ^{75}As and ^{79}Br where the high-lying negative-parity bandheads decay to both the lower-lying positive and negative-parity levels of the neighboring band structures, the bandhead of band-5 of ^{77}As is found to decay only to the positive-parity bands, and no decay path is observed that feeds the low-lying negative-parity levels of band-3.

The onset of possible shape at the regime of bandhead energy of band-5 is also investigated using TRS calculations. The calculations have been performed on the basis of the negative-parity positive-signature framework and at the rotational frequency of $\hbar\omega = 0.35$ MeV. The calculated results suggest for a near prolate shape having $\gamma \approx -15^\circ$ and $\beta_2 \approx 0.21$ (see Fig. 13).

As can be seen from Fig. 3, the level spacing between the consecutive levels of band-5 gradually increases up to $23/2^{(-)}$, 4477 keV level. Beyond the $23/2^{(-)}$ level, the change in the level spacing does not follow the same trend. This observation indicates the onset of a different configuration after the $23/2^{(-)}$, 4477 keV level. Hence, we would consider

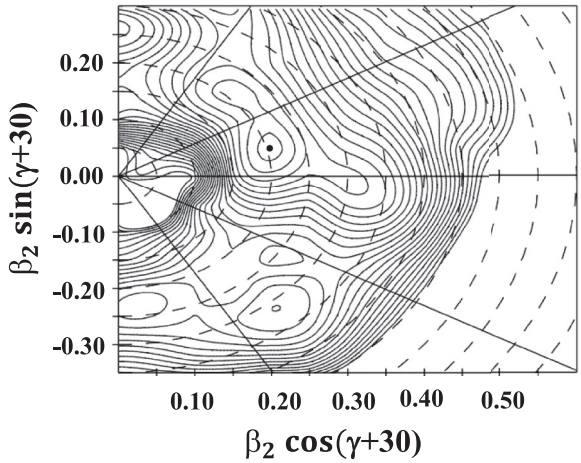

FIG. 13. The contour plot as obtained from the TRS calculations. The plot corresponds to the bandhead regime of band-5 with $\hbar\omega = 0.35$ MeV. The plot has been made by maintaining an energy difference of 0.25 MeV between the two consecutive contours.

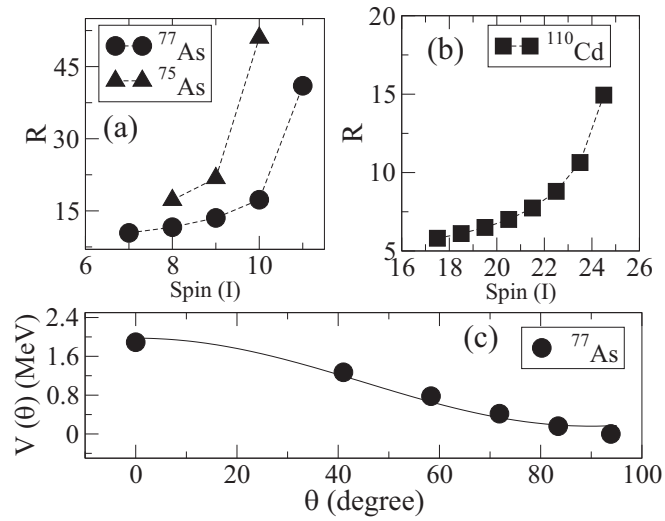

FIG. 14. The rate of variation of shear angle θ as a function of spin I for the nuclides (a) ^{75,77}As and (b) ^{110}Cd. A mark difference in the variation profile at the highest observed spin regime can clearly be seen from plots (a) and (b) (see text for details). The dashed lines connecting the data points have been drawn to guide the eye. (c) The effective interaction strength $V(\theta)$ among the proton and neutron angular-momentum vectors belonging to the shear blades plotted as a function of shear angle θ. The solid line is the fit to the experimental data following the prescription as discussed in Ref. [44].

only the band members in between $13/2^-$ to $23/2^{(-)}$ for the subsequent discussion.

Furthermore, the underlying structure of band-5 has been investigated by the use of semiclassical approach of Macchiavelli *et al.* [44,45]. In this approach, the observed bandhead spin is generated by the perpendicular coupling of proton angular momentum (j_π) and neutron angular momentum (j_ν). In the present work, the bandhead spin $13/2^-$ of band-5 has been reproduced by assuming $j_\pi = 4.5\hbar$ and $j_\nu = 5.0\,\hbar$. The contribution of the core rotation in the experimentally observed spin is determined by considering a value of $\Delta R/\Delta I = 0.4$. Under this consideration, shears angles have been calculated for each spin of the members of band-5.

The rate of variation of the calculated shear angles θ as a function of spin I is shown in Fig. 14(a). The parameter, R ($= d\theta/dI$) and the corresponding I values are extracted following the prescription:

$$R = \frac{d\theta}{dI} = \frac{\theta_1 - \theta_2}{I_1 - I_2}, \tag{3}$$

where the shear angles θ_1 and θ_2 are associated with spin members I_1 and I_2, respectively:

$$I = \frac{I_1 + I_2}{2}. \tag{4}$$

Figure 14(a) also depicts the extracted variation profile for the high-lying negative-parity band members of ^{75}As. As is obvious from the figure, both ^{75,77}As exhibit the similar type of varying trend. Figure 14(b) shows the calculated profile for ^{110}Cd, where the presence of shear band has been firmly established from the previous study [45]. The effective interaction strength between the two blades of the shear for ^{77}As is calculated following the standard methodology prescribed in Ref. [44]. In Fig. 14(c) we have shown the variation of the effective interaction strength [$V(\theta)$] between the two blades as a function of shears angle θ. The experimental level energies are found to be best reproduced for a value of $V_2 = 1.209$ MeV. Thus, the calculated interaction strength (V_2) per pair is ≈604 keV.

As suggested in Refs. [2,7,46], the shear angle varies smoothly with spin for the shear mechanism. But the feature for the onset of stapler mechanism is that the shear angle falls rapidly as the band approaches the highest spin value due to the closing of shears angle. Figures 14(a) and 14(b) clearly demonstrate this variance. The extracted value of R for ^{110}Cd is about four units as the well-established positive-parity shears band in ^{110}Cd approaches the maximally observed spin value. A value of about 30 units has been found for R in the case of ^{75}As [see Fig. 14(a)] as the previously observed high-lying negative-parity stapler band approaches the highest observed spin. The onset of stapler mechanism in the negative-parity band structure of ^{75}As has been explained on the basis of the TAC-CDFT calculation [7]. In the case of ^{77}As, the extracted value of R attains a value of 24 units [see Fig. 14(a)] as the observed negative-parity band (band-5 of Fig. 3) structure gains the maximal angular momentum. As can be seen from Figs. 14(a) and 14(c), the variation profile for band-5 of ^{77}As exhibits a notable deviation in comparison to that of the shear band structure of ^{110}Cd; whereas a remarkable similarity persists among the band structures of ^{75,77}As. This comparison suggests for the possible persistence of stapler-like mechanism in generating the high-lying negative band structure (band-5) of ^{77}As. In the presence of moderate triaxilarity, it is expected that the tilted angle (the angle between the symmetry axis and total spin I) should increase faster in comparison to that for a completely axially symmetric nucleus. As discussed in Ref. [47], the

onset of faster growth of the tilted angle should give rise to the rapid fall of $B(M1)$ values with the increasing value of spin I. However, in the absence of the experimental $B(M1)$ values, the said feature could not be examined in the present investigation for ^{77}As.

V. CONCLUSIONS

The low and medium spin level structure of ^{77}As has been investigated in the present work using the spectroscopic data obtained from the ^{76}Ge$(\alpha, p2n)$ fusion evaporation reaction at the incident-beam energy of 40 MeV. The level scheme has been extended up to the excitation energy of $E_x \approx 7.5$ MeV and spin of $J = 33/2\,\hbar$. The band crossing phenomena, at the frequency regime of $\hbar\omega \approx 0.65$ MeV, due to $\nu(g^2_{9/2})$ alignment has been observed in the yrast positive-parity band structure built on the isomeric $9/2^+$ state. The presence of triaxial shape before and after the band crossing regime has been demonstrated following the results from the TRS calculations. The experimentally observed large signature splitting of the signature partner bands have been discussed within the framework of particle plus triaxial rotor model and shell-model calculations. The shell-model calculations have been carried out using the fpg model space and jj44b, JUN45 interactions. It appears that the results from JUN45 calculations provide an overall better prediction in comparison to that from jj44b calculations. A quasi-γ vibrational band has been found to develop on the nonyrast $13/2^+$ state. The evidence for the possible onset of stapler like mechanism in the observed high-lying negative-parity dipole band has been presented. The results from the present and previous investigations [2,7,46] provide a tantalizing hint towards the systematic occurrence of stapler mechanism for generating the angular momenta in the high-lying negative-parity band structures in $A \approx 80$ region. However, the knowledge of $B(M1)$ transition rates of the concerned transitions are very much required for proper characterization of the observed band structures. This warrants further experimental and theoretical investigations.

ACKNOWLEDGMENTS

The help and cooperation received from all the participants for their joint effort in setting up the INGA facility at VECC, Kolkata is highly appreciated. Thanks are due to the cyclotron operating staff of VECC, Kolkata for providing good quality alpha beams. The assistance received from the laboratory staff at VECC, Kolkata in preparing the targets is gratefully acknowledged. Financial support from the Department of Science and Technology (D.S.T.), Government of India (Grant No. IR/S2/PF-03/2003-II) is also gratefully acknowledged. One of the authors (A.C.) would like to sincerely thank Science and Engineering Research Board (SERB), Government of India (File No. CRG/2021/004680), Inter-University Accelerator Centre (IUAC), New Delhi, India (UFR Project Code No. 71344), and UGC-DAE Consortium for Scientific Research (UGC-DAE CSR), India (Project no. CRS/2021-22/02/472) for providing the necessary financial assistance in carrying out this collaborative research work. One of the authors (S.C.) acknowledges the financial assistance received from the Science and Engineering Research Board (SERB, India), under National Post-Doctoral Fellowship (NPDF) scheme vide reference no. PDF/2022/001829.

[1] I. Ray *et al.*, Nucl. Phys. A **646**, 141 (1999).
[2] A. K. Mondal *et al.*, Phys. Rev. C **102**, 064311 (2020).
[3] M. K. Raju, P. V. M. Rao, S. K. Tandel, P. Sugathan, R. P. Singh, S. Muralithar, T. S. Reddy, B. V. T. Rao, J. Meng, S. Zhang, J. Li, Q. B. Chen, B. Qi, and R. K. Bhowmik, Phys. Rev. C **92**, 064324 (2015).
[4] J. Döring, G. D. Johns, R. A. Kaye, K. W. Kemper, H. Sun, G. N. Sylvan, and S. L. Tabor, Phys. Rev. C **53**, 2674 (1996).
[5] H. Schnare *et al.*, Phys. Rev. Lett. **82**, 4408 (1999).
[6] S. Frauendorf, Nucl. Phys. A **557**, 259 (1993).
[7] C. G. Li *et al.*, Phys. Lett. B **766**, 107 (2017).
[8] R. R. Betts, S. Mordechai, D. J. Pullen, B. Rosner, and W. Scholz, Nucl. Phys. A **230**, 235 (1974).
[9] M. Schrader, H. Reiss, G. Rosner, and H. V. Klapdor, Nucl. Phys. A **263**, 193 (1976).
[10] G. Rotbard, M. Vergnes, J. Vernotte, G. Berrier-Ronsin, J. Kalifa, and R. Tamisier, Nucl. Phys. A **401**, 41 (1983).
[11] B. P. Kay *et al.*, Phys. Rev. C **79**, 021301(R) (2009).
[12] R. N. Cherry Jr. and M. L. Wiedenbeck, Nucl. Phys. A **252**, 445 (1975).
[13] R. D. Meeker and A. B. Tucker, Nucl. Phys. A **157**, 337 (1970).
[14] E. M. Lent, Ph.D. thesis, University of California, 1974 (unpublished).
[15] A. J. Kestelman, M. A. Arribére, I. M. Cohen, E. Achterberg, and J. C. Furnari, Phys. Rev. C **61**, 067304 (2000).
[16] G. Meierhofer, P. Grabmayr, L. Canella, P. Kudejova, J. Jolie, and N. Warr, Eur. Phys. J. A **48**, 20 (2012).
[17] S. Das *et al.*, Nucl. Instrum. Methods Phys. Res., Sect. A **893**, 138 (2018).
[18] D. C. Radford, Nucl. Instrum. Methods Phys. Res., Sect. A **361**, 297 (1995).
[19] J. Theuerkauf, S. Esser, S. Krink, M. Luig, N. Nicolay, O. Stuch, and H. Wolters, computer code Tv, Institute for Nuclear Physics, University of Cologne, 1993 (unpublished).
[20] A. Krämer-Flecken, T. Morek, R. M. Lieder, W. Gast, G. Hebbinghaus, H. M. Jäger, and W. Urban, Nucl. Instrum. Methods Phys. Res., Sect. A **275**, 333 (1989).
[21] M. A. Jones, W. Urban, and W. R. Phillips, Rev. Sci. Instrum. **69**, 4120 (1998).
[22] E. S. Macias, W. D. Ruhter, D. C. Camp, and R. G. Lanier, Comput. Phys. Commun. **11**, 75 (1976).
[23] R. Chakrabarti *et al.*, Phys. Rev. C **80**, 034326 (2009).
[24] S. Chakraborty *et al.*, Phys. Lett. B **811**, 135854 (2020).
[25] W. Nazarewicz, J. Dudek, R. Bengtsson, T. Bengtsson, and I. Ragnarsson, Nucl. Phys. A **435**, 397 (1985).
[26] W. Nazarewicz, M. A. Riley, and J. D. Garrett, Nucl. Phys. A **512**, 61 (1990).
[27] S. Chakraborty *et al.*, Phys. Rev. C **107**, 064318 (2023).
[28] D. Lieberz *et al.*, Phys. Lett. B **282**, 7 (1992).
[29] M. A. J. Mariscotti, Gertrude Scharff-Goldhaber, and Brian Buck, Phys. Rev. **178**, 1864 (1969).
[30] S. M. Harris, Phys. Rev. **138**, B509 (1965).

[31] T. Bengtsson and I. Ragnarsson, Nucl. Phys. A **436**, 14 (1985).
[32] S. E. Larsson, Phys. Scr. **8**, 17 (1973).
[33] S. E. Larsson, G. Leander, and I. Ragnarsson, Nucl. Phys. A **307**, 189 (1978).
[34] A. D. Ayangeakaa *et al.*, Phys. Rev. Lett. **123**, 102501 (2019).
[35] A. D. Ayangeakaa *et al.*, Phys. Rev. C **107**, 044314 (2023).
[36] H. Toki and A. Faessler, Phys. Lett. B **63**, 121 (1976).
[37] I. Wakudyanaye, Ph.D. thesis, University of the Western Cape, 2022, Chap. 3, p. 26.
[38] P. B. Semmes and I. Ragnarsson, *Future Directions in Nuclear Physics with* 4π *Gamma Detection Systems, Strasbourg, France*, AIP Conf. Proc. No. 259 (AIP, New York, 1991), p. 566.
[39] R. Banik *et al.*, Phys. Rev. C **101**, 014322 (2020).
[40] V. Kumar, P. C. Srivastava, and I. O. Morales, Mod. Phys. Lett. A **30**, 1550093 (2015).
[41] B. A. Brown and W. D. M. Rae, Nucl. Data Sheets **120**, 115 (2014).
[42] Y. Toh *et al.*, Phys. Rev. C **87**, 041304(R) (2013).
[43] S. Chakraborty *et al.*, J. Phys. G **47**, 095104 (2020).
[44] A. O. Macchiavelli, R. M. Clark, P. Fallon, M. A. Deleplanque, R. M. Diamond, R. Krücken, I. Y. Lee, F. S. Stephens, S. Asztalos, and K. Vetter, Phys. Rev. C **57**, R1073 (1998).
[45] R. M. Clark *et al.*, Phys. Rev. Lett. **82**, 3220 (1999).
[46] C. G. Li *et al.*, Phys. Rev. C **100**, 044318 (2019).
[47] A. A. Pasternak *et al.*, Eur. Phys. J. A **37**, 279 (2008).
[48] https://www-nds.iaea.org/public/ensdf_pgm/.